

Received: 2017.01.22
Accepted: 2017.02.26
Published: 2017.08.31

Nanomechanical Characteristics of Cervical Cancer and Cervical Intraepithelial Neoplasia Revealed by Atomic Force Microscopy

Authors' Contribution:
Study Design A
Data Collection B
Statistical Analysis C
Data Interpretation D
Manuscript Preparation E
Literature Search F
Funds Collection G

ABCDEF 1 **Yueyi Cui***
BCDF 2 **Xuejie Zhang***
B 1 **Ke You**
B 1 **Yanli Guo**
C 3 **Congrong Liu**
AG 2 **Xiaohong Fang**
AEG 1 **Li Geng**

1 Department of Obstetrics and Gynecology, Peking University 3rd Hospital, Beijing, P.R. China
2 Key Laboratory of Molecular Nanostructures and Nanotechnology, Institute of Chemistry, Chinese Academy of Sciences, Beijing, P.R. China
3 Department of Pathology, Peking University Health Science Center, Beijing, P.R. China.

* These authors contributed equally to this work

Corresponding Authors:

Li Geng, e-mail: gengli1957@bjmu.edu.cn, Xiaohong Fang, e-mail: xfang@iccas.ac.cn

Source of support:

This study was supported by grants from the National Natural Science Foundation of China (81472429, 21127901) and the National Basic Research Program of China (973 Program, 2014CBA02003, 2013cb933701)

Background: Understanding the biological features and developmental progress of cervical cancer is crucial for disease prevention. This study aimed to determine the nanomechanical signatures of cervical samples, ranging from cervicitis to cervical carcinomas, and to investigate the underlying mechanisms.

Material/Methods: Forty-five cervical biopsies at various pathological stages were subjected to atomic force microscopy (AFM) measurements. Cdc42 and collagen I were quantified using immunohistochemical staining to investigate their relationship with nanomechanical properties of cervical cancers and premalignant lesions.

Results: We found that the lower elasticity peaks (LEPs) in the high-grade squamous intraepithelial lesion (HSIL) group (21.24 ± 3.83 kPa) and higher elasticity peaks (HEPs) in the cancer group (81.23 ± 8.82 kPa) were upshifted compared with the control group (LEP at 8.51 ± 0.18 kPa and HEP at 44.07 ± 3.54 kPa). Furthermore, compared with the control [29.51 ± 13.61 for cell division cycle 42 (Cdc42) expression and 28.61 ± 17.65 for collagen I expression], immunohistochemical staining verified a significant increase of Cdc42 in the HSIL group (50.57 ± 23.85) and collagen I (56.09 ± 25.70) in the cancer group. In addition, using the Pearson correlation coefficient, Cdc42 expression tended to be positively correlated with LEP locations ($r=0.63$, $P=0.012$), while collagen I expression displayed a strong and positive correlation with HEP positions ($r=0.88$, $P<0.001$).

Conclusions: The nanomechanical properties of HSIL and cancer biopsies show unique features compared with controls, and these alterations are probably due to changes in cytoskeleton and extracellular matrix contents.

MeSH Keywords: **cdc42 GTP-Binding Protein • Cervical Intraepithelial Neoplasia • Collagen Type I • Microscopy, Atomic Force • Uterine Cervical Neoplasms**

Full-text PDF: <https://www.medscimonit.com/abstract/index/idArt/903484>

 3213   4  46



Background

Cervical cancer is the one of the most common cancers in women worldwide, with approximately 500 000 cases each year [1]. As the most prevalent cancer affecting women in many developing countries [2], it causes death when women are still raising a family at a comparably young age, driving underprivileged households into deeper poverty [3]. Along with its severe social influence, cervical cancer has distinguishing biological features. It is well accepted that cervical cancer is presumably preceded by precursor lesions in most cases [4]. In addition, the existence of the premalignant stage, also known as cervical intraepithelial neoplasia (CIN), makes cervical cancer a theoretically preventable disease [5], thus highlighting the importance of understanding the biological processes of cervical cancer progression.

Physical and chemical factors mediate cell fate and behavior in tissues, such as proliferation, differentiation, and migration [6,7]. Recently, the role of mechanical force and physical interactions and their interplay with cancer progression has drawn extensive attention [8]. Researchers have applied various types of analytical techniques to measure the nanomechanical properties of cancer cells, such as micropipette aspiration [9], magnetic twisting cytometry [10], optical tweezers [11], and atomic force microscopy (AFM) [12,13]. Most studies using AFM have characterized increased elasticity and compliance as nanomechanical properties of tumor cells in clinical samples [14,15] and cancer cell lines derived from various cancers [16], including kidney [12], bladder [17], ovarian [18], and cervical [19] cancers, although controversies remain concerning melanoma and cervical carcinoma [20,21]. However, there was a lack of holistic biomechanical profiles of cancer until Plodinec and colleagues resolved the nanomechanical signature of breast cancer using indentation-type AFM in 2012 [22]. Recently, the mechanical properties of liver cancer tissue have been quantified at the nanoscale [23]. Nevertheless, there has been no reports on nanomechanical features of cervical cancer so far, despite the fact that cervical cancer falls into the squamous cell carcinoma category and is characterized by the unique precedence of dysplastic lesions, both of which are quite different from breast cancer (adenocarcinoma) and liver cancer (hepatocellular carcinoma) [23]. Hence, it is crucial to reveal the mechanical characteristics of cervical cancer and precancerous lesions.

The cellular tumor suppressor P16^{INK4a} has been identified as a marker of infection by human papilloma virus [24], thus being viewed as a sensitive indicator of the severity of cervical lesions. Cdc42 is a member of the Rho family and participates in controlling the actin cytoskeleton architecture [25], which serves as a cytoskeleton marker. Collagen I is the major component of extracellular matrix (ECM) in cervical tissue [26,27],

giving it rigidity [28]. According to previous studies [24–28], immunohistochemical (IHC) staining can be applied to assess the expressions of P16^{INK4a}, Cdc42, and collagen I.

In this study, we aimed to determine the comprehensive nanomechanical properties of cervical cancer and precancerous lesions, and to preliminarily investigate the mechanism of their alterations compared to control tissue. To achieve this aim, we measured elasticity distributions of cervical tissue samples at various pathological stages using AFM. We also quantified cell division cycle 42 (Cdc42) and collagen I expression using immunohistochemical (IHC) staining to evaluate alterations in the cytoarchitecture and extracellular matrix (ECM). Finally, to confirm their roles, we analyzed the relationship between representative Cdc42 and collagen I expression and nanomechanical indexes.

Material and Methods

Cervical biopsies and sample preparation

Human cervical biopsies were collected from the outpatient gynecologic clinic, Department of Obstetrics and Gynecology, Peking University Third Hospital from April 2015 to January 2016. Participants were included in the study for their abnormal cervical cytological findings or positive results in high-risk HPV test, or being suspected of cervical cancer or precancerous lesions clinically. The Ethics Committee of Peking University Third Hospital approved the study, and informed consent was obtained from all participants included in the study. Cervical biopsies were surgically removed using forceps under colposcopy from each participant. The biopsy samples, shaped as an irregular cylinder with diameters ranging from 2 to 6 mm, were immediately transferred to precooled lactated Ringer's solution (Leagene Co. Ltd, China) containing anhydrous glucose (50 g/L) and a protease inhibitor cocktail (1 tablet/50 mL; Pierce, Thermo Scientific, NY), and stored at 4°C for no more than 72 h until AFM analysis [22].

AFM measurement and data analysis

Each sample was immobilized on a 35-mm dish (Corning, NY) using 1-minute™ biocompatible epoxy gel (Devcon, MA). To avoid interfering with the sample's mechanical properties, the manipulation was performed as gently as possible. Immediately after the specimens were glued to the dishes (1–1.5 min), they were submerged in the buffer solution (lactated Ringer's solution containing anhydrous glucose and the protease inhibitor cocktail) until completion of AFM (Figure 1A).

All AFM measurements were carried out on a Bioscope™ Catalyst™ AFM (Veeco, CA) (Figure 1B) at room temperature,

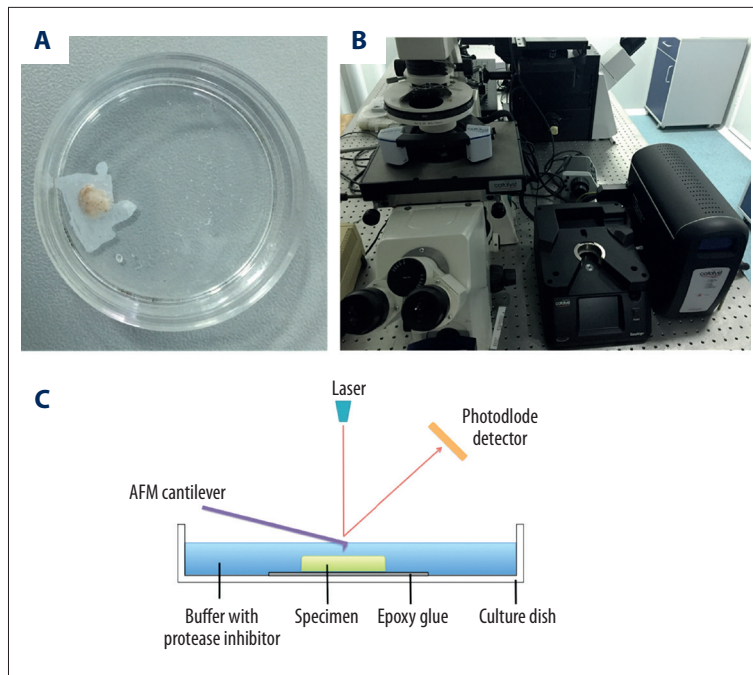


Figure 1. Measurement of the nanomechanical properties of cervical biopsies using AFM. **(A)** Top view of an immobilized cervical biopsy in Ringer's solution for AFM measurement. **(B)** Image of Bioscope™ Catalyst™ AFM. **(C)** Schematic illustration of AFM measurement of cervical tissue samples.

while the curves were obtained under “Contact Mode in Fluid”. A schematic diagram of the AFM experiment is shown in Figure 1C. Si_3N_4 cantilevers (DNP-10; Bruker, Germany) were used when a tip B (nominal spring constant: $k=0.06\text{N/m}$, resonance frequency (air): $f=18\text{--}65\text{ kHz}$, tip length: $8.0\ \mu\text{m}$, tip radius= $20\ \text{nm}$, and side angle $\theta=17.5\pm 2.5^\circ$) was used for this experiment. To minimize systemic error, all samples were measured using the same tip, cleaned by plasma cleaner (Harrick Scientific, NY) before the next use. The spring constant k was calibrated using Nano Scope Analysis software (Bruker) and the thermal fluctuation method before each experiment. The deflection sensitivity was established in buffer using $22\times 22\text{-mm}$ glass coverslips as the infinitely stiff reference material. The cantilever with tip B was initially positioned above the specimen under an optical microscope, followed by gently moving onto the tissue surface. The maximum loading force was set to $1\text{--}1.4\ \text{nN}$, while the frequency of the load/unload cycle was $0.5\ \text{Hz}$. Then, we collected 1500 force-distance curves from each sample and analyzed them using a user-defined program in Matlab (MathWorks, MA), after which quality control was implemented, including denoising curves by the convolution operation and removing disturbance on the deflection signals caused by beam vibration. Generally, only 800–1200 force curves were valid curves in each sample after quality control. The contact point of the AFM tip with the tissue surface was determined by the difference operation. We obtained force curves of a 3-mm-thick gel alone following the same method in case they were mistakenly recognized as force curves from the samples. The elasticity modulus was calculated based on the Hertz model [15], and the practical algorithm was determined as follows [23]:

$$F = \frac{2}{\pi} \times \tan \alpha \times \frac{E}{1-\nu^2} \times \delta^2 \quad (1)$$

where F represents the load force of the cantilever, α is the half angle of the tip, E refers to the Young's modulus of the tissue, ν is the Poisson ratio, and δ indicates the tissue indentation depth. In this experiment, we chose $\alpha=18^\circ$ and $\nu=0.5$ for the calculation.

Histopathology and IHC

Specimens were fixed in 4% paraformaldehyde overnight and then embedded in paraffin following standard histological procedures. Cervical tissues were sequentially sectioned at 5-mm thicknesses with the first and last sections stained by hematoxylin and eosin. Histopathological diagnoses and grading, including cervicitis, CIN 1, CIN 2, CIN 3, and cervical cancer, were independently performed by 2 qualified experienced pathologists.

To explore the possible mechanism underlying the nanomechanical changes, the expression of $\text{P16}^{\text{ink4A}}$, collagen I, and Cdc42 were assessed by IHC staining. Briefly, paraffin-embedded sections were deparaffinized by submerging in dimethylbenzene and then rehydrated in an ethanol dilution series before heat-induced epitope retrieval in citric acid buffer. After blocking endogenous peroxidase activity, the sections were incubated with anti- $\text{P16}^{\text{ink4A}}$ (1: 80; ZSGB-Bio, China), anti-Cdc42 (1: 300, Santa Cruz Biotechnology, CA), and anti-collagen I (1: 200, Epitomics, UK) antibodies at 4°C overnight. Then, the specimens were incubated with horseradish peroxidase-conjugated secondary antibodies at 37°C for 60 min, after which

a diaminobenzidine kit (ZSGB-Bio) was used for visualization. To ensure the accuracy of positive staining scores, none of the specimens were counterstained until determination of their integrated optical density (IOD) values, after which the specimens were immersed in dimethylbenzene again to remove the mounting medium and coverslips, rehydrated in the ethanol dilution series, and finally counterstained.

IHC quantitation and image analysis

IHC staining of tissue sections was scanned for subsequent quantitative analysis using a NanoZoomer Digital Pathology System (Hamamatsu, Japan) that simultaneously provided high resolution images and a stable external light source [29]. The digital images in their original NDPI file format were converted to the TIFF format when 5 fields of each specimen were randomly selected at $\times 200$ magnification (zoom factor: 20). The image analysis was conducted using Image Pro Plus 6.0. A positive intensity was quantified and represented by the formula $(\text{IOD}/\text{area}) \times 1000$ [30,31]. We measured IOD values using IHC images without counterstained nuclei, while measuring total areas using IHC images with counterstaining.

Statistics

Individual elasticity values for each specimen were summed in Origin (OriginLab, MA) to obtain the distribution of elasticity values. The counts were normalized according to the total elasticity values per specimen. Gaussian or multi-peak fittings were performed to observe peak locations and the elasticity distribution of each sample. All individual elasticities for each group (grouping criteria is described later in this article) were pooled to obtain an overview of the characteristics of the disease stage. The histogram bin widths of non-cancer groups (control and high-grade squamous intraepithelial lesion; HSIL) and the cancer group were set to 1 and 10 kPa, respectively. Results are represented as the means \pm standard deviations. Statistical analyses were performed using one-way analysis of variance with post hoc testing by Fisher's LSD multiple comparison test. Correlations between representative individual sample peak locations and $(\text{IOD}/\text{area}) \times 1000$ values were quantified using Pearson's correlation coefficients in SPSS 13.0 (IBM Cop., NY). Statistical significance was set at $P < 0.05$.

Results

General distribution of the biopsies and grouping

In total, we obtained 45 human cervical specimens, including 2 cases of cervicitis, 13 cases of CIN1, 10 cases of CIN2, 6 cases of CIN2-3, 8 cases of CIN3, and 6 cases of cervical carcinomas (CIN2-3 refers to CIN2 with focal CIN3). Because CIN1 is

distinguished from CIN2 and 3 in terms of biological progression and clinical prognosis [32,33] and is recommended to only undergo rescreening within 3 years according to World Health Organization guidelines [34], they were regarded as the "control group" together with cervicitis. In fact, cervicitis and CIN1 demonstrated similar nanomechanical characteristics (data not shown) in this study. Similarly, based on the fact that CIN2, CIN2-3, and CIN3 undergo similar progressive development and share a common therapeutic regimen [34,35], they were regarded as a single group (HSIL). In addition, they showed analogical elasticity distributions (data not shown). The "cancer group" consisted of the other 6 cases of cervical carcinomas.

Nanomechanical properties of human cervical biopsies

Because the elasticity of the epoxy gel greatly exceeded (peaked at 66.3 ± 0.41 MPa) that of the sample, we could essentially rule out the possibility that the epoxy gel directly interfered with the sample AFM measurement. In general, although we also observed minor platykurtic peaks in control and cancer groups due to precise curve fitting, the accumulated nanomechanical force distribution of all 3 groups manifested 2 prominent major peaks (Figure 2). The 2 distinguishing peaks in the control group were located at 8.51 ± 0.18 kPa (lower elasticity peak; LEP) and 44.07 ± 3.54 kPa (higher elasticity peak; HEP) (Figure 2). Although the distribution of HEPs indicated greater heterogeneity across the samples in the HSIL group, it centered at exactly the same position (43.60 ± 9.42 kPa) as in the control group. However, the LEP in the HSIL group was observed at 21.24 ± 3.83 kPa, which shifted to a markedly higher location compared with the controls (Figure 2). More interestingly, although the LEP in the cancer group (8.82 ± 2.05 kPa) exhibited similar characteristics as in the controls, its HEP (81.23 ± 8.82 kPa) was significantly stiffer than the controls (Figure 2).

Expression changes of P16^{ink4A}, Cdc42, and collagen I during cervical cancer progression

According to previous studies, LEP and HEP correspond to cellular elasticity and ECM rigidity, respectively [22,36]. To investigate the mechanisms underlying the alteration of nanomechanical properties, we evaluated the expression of Cdc42 and collagen I by IHC staining, which are a cytoskeleton marker and major ECM component, respectively. Disease progression was demonstrated by P16^{ink4A} expression (Figure 3). In agreement with our speculation, Cdc42 expression was significantly increased in the HSIL group (50.57 ± 23.85 , $P < 0.01$), but we did not detect a remarkable difference between control (29.51 ± 13.61) and cancer (29.37 ± 16.92) groups (Figure 3). Similarly, collagen I was significantly upregulated in the cancer group (56.09 ± 25.70 , $P < 0.01$) compared with non-cancer groups, while there was no statistical difference between control (28.61 ± 17.65) and HSIL (31.04 ± 21.37) groups (Figure 3).

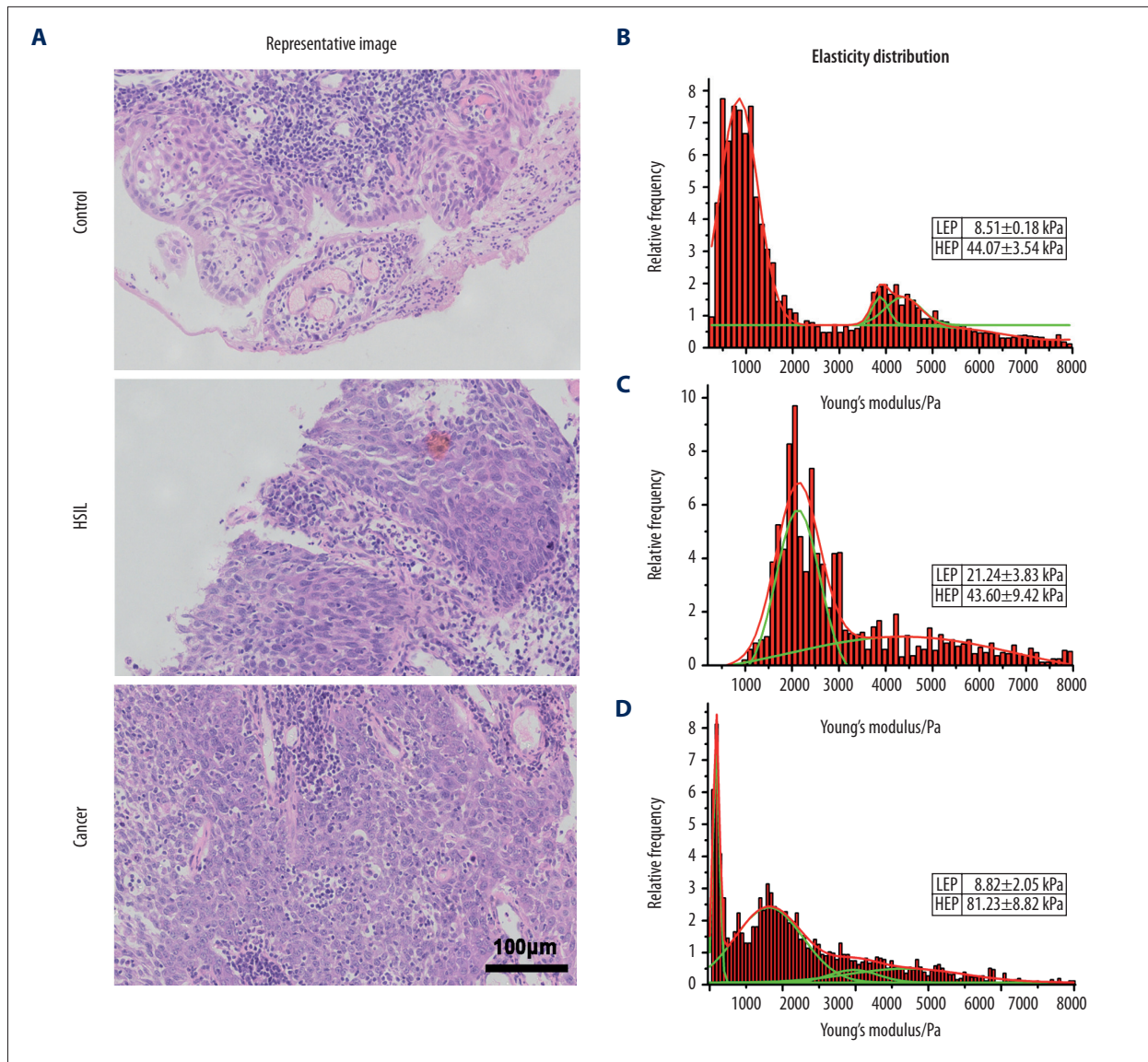


Figure 2. Elasticity distribution of cervical biopsies. **(A)** Representative images of various stages of cervical lesions and the right panel is the corresponding stiffness distribution (Scale bars: 100 µm). **(B)** Two distinguishing peaks were identified at 8.51 ± 0.18 kPa (LEP) and 44.07 ± 3.54 kPa (LEP) in the control group. **(C)** LEP in the HSIL group shifted up to 21.24 ± 3.83 kPa, while its HEP location (43.60 ± 9.42 kPa) was approximately the same as in the controls. **(D)** LEP in the cancer group (8.82 ± 2.05 kPa) did not show visible differences from the controls, while its HEP shifted upward (81.23 ± 8.82 kPa) compared with the controls.

The HSIL LEP upshift was correlated with Cdc42 upregulation when the cancer HEP upshift was related to increased expression of collagen I. To further establish that cytoarchitecture and ECM alterations contributed to the nanomechanical characteristic changes of HSIL and cervical cancer, we next investigated their correlations with elasticity distribution peak locations. Only samples exhibiting a representative bimodal elasticity distribution were chosen for analysis. We found that the expression of Cdc42 had a clear tendency to be positively correlated with representative LEP locations ($r=0.63$, $P=0.012$) (Figure 4A), which was consistent with the assumption that

the HSIL LEP upshift was due to the cytoskeleton alteration. Similarly, representative HEP locations showed a strong positive correlation with collagen I expression ($r=0.88$, $P<0.001$) (Figure 4B), indicating that cancer HEP upshifts should probably be attributed to the increase in collagen I content.

Discussion

AFM has been widely used in nanomechanical studies because of its high resolution in force determination [11–22,37]. Several

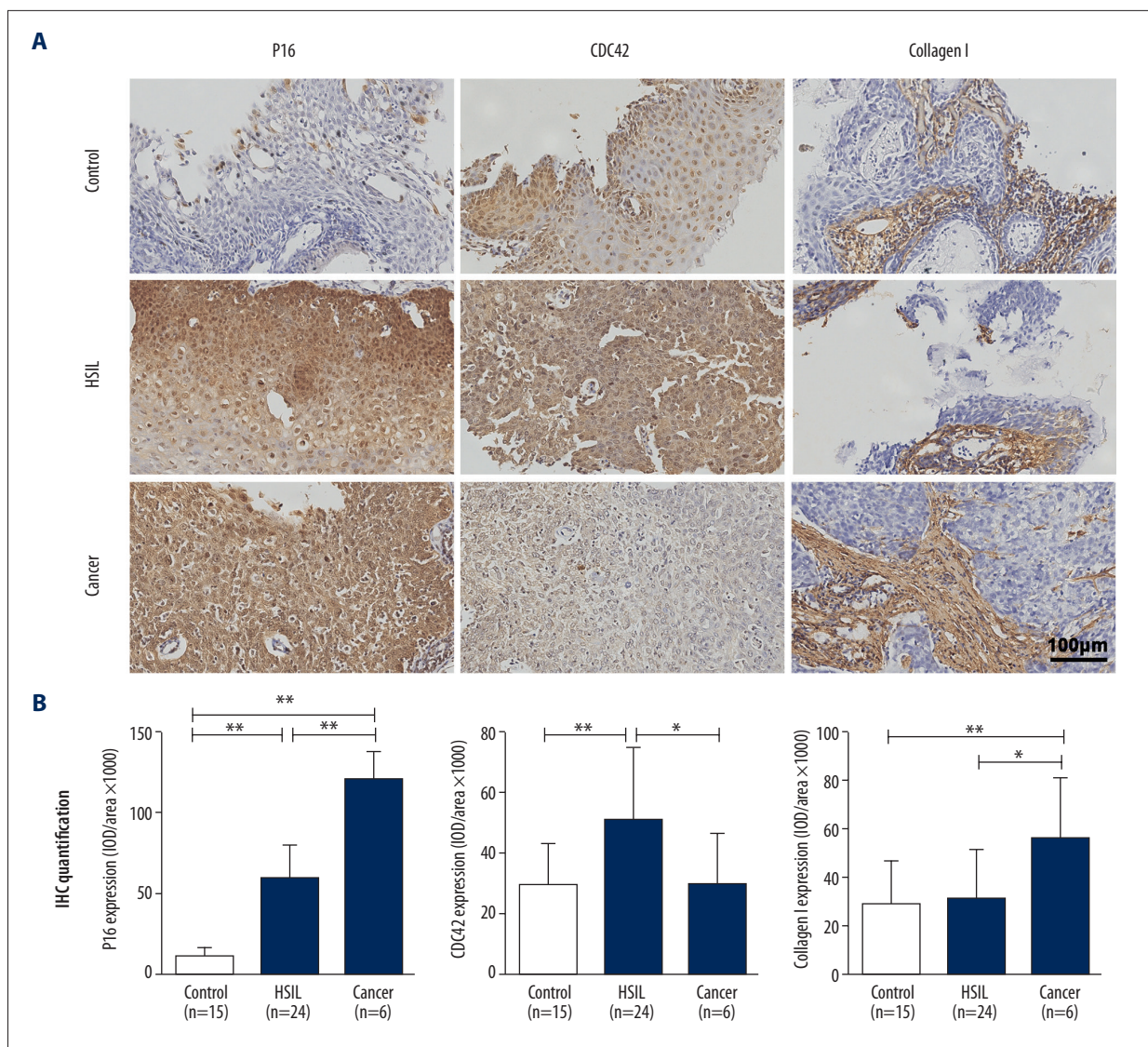


Figure 3. IHC staining of P16ink4A, Cdc42, and collagen I in cervical biopsies. **(A)** Representative IHC images of P16, Cdc42, and collagen I in control, HSIL, and cancer groups. (Scale bars: 100 µm). From left to right: P16, Cdc42, and collagen I; from top to bottom: control, HSIL, and cancer groups. **(B)** Quantification of P16, Cdc42, and collagen I expression in each group. From left to right: P16, Cdc42, and collagen I (* P<0.05, ** P<0.01).

studies, including our own, have performed mechanical characterization of cervical squamous carcinoma cells [19,20,38]. However, to date, the comprehensive mechanics of cervical cancer biopsies at the nanoscale are unknown. In this study, we obtained the comprehensive nanomechanical distributions of cervical tissues including cancer samples, and preliminarily investigated the underlying molecular mechanisms.

We found several intriguing characteristics of the elasticity distribution in cervical biopsies using AFM. First, our data revealed that cervical cancer exhibited a typical bimodal distribution that had a similar nanomechanical signature as breast cancer and hepatocellular carcinoma [22,23]. In addition, the

location of the cervical cancer HEP was approximately 2-fold higher than that of control and HSIL groups, as reported previously [22,23], although the absolute values of the samples were greater than those in other studies, which could be caused by various factors such as gel use, AFM parameter settings, and sample ingredients [39]. Second, 2 elasticity distribution peaks were also observed in non-cancer groups when all force curves within each group were pooled. This result is reasonable because the unimodal stiffness distribution of control and benign tissues in other studies was obtained from representative individual samples [22,23], and there was a considerable percentage of unimodal elasticity distribution in individual cases in our study. Moreover, a higher proportion of

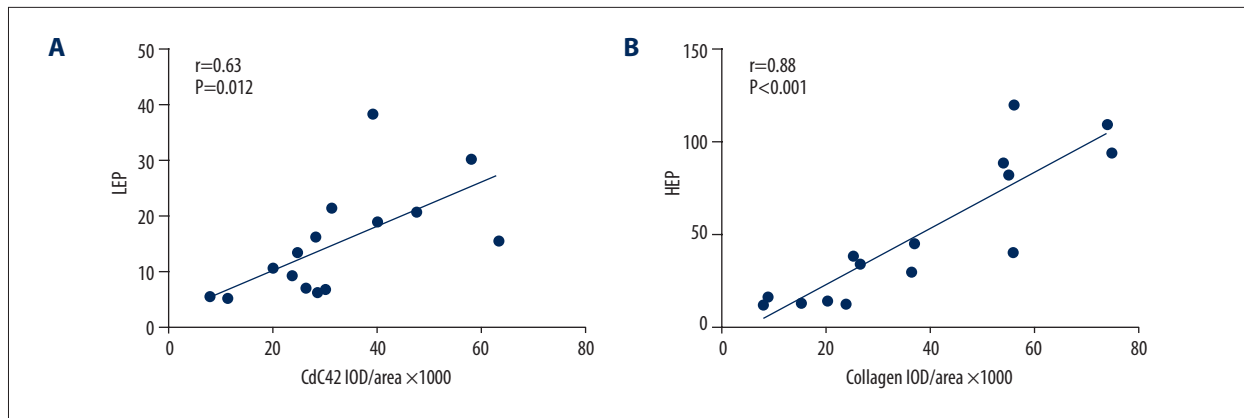


Figure 4. Correlation analysis between LEP and Cdc42 expression, and between HEP and collagen I expression. (A) Pearson's correlation indicated that LEP and Cdc42 IOD/area values showed a significant positive tendency of correlation ($r=0.63$, $P=0.012$). (B) Correlation analysis verified a close positive correlation between HEP and collagen I IOD/area values ($r=0.88$, $P<0.001$).

ECM (such as collagen I verified by IHC staining) in cervical biopsies might contribute to the specific phenotype. Lastly, the cancer LEP did not show a visible difference compared with the control LEP. However, considering the heterogeneity and force curve quantity in this study, it remains to be confirmed whether this was indeed the case or was the result of relatively few cancer samples or even a system or random error.

The most remarkable finding in our study was that LEP in the HSIL group and HEP in the cancer group shifted to a higher position compared with the corresponding elasticity distribution peaks in the control group, establishing that cell rigidity in HSIL and ECM stiffness of cancer were greater than those in the controls. The shifts resembled the trend in the elasticity alteration of benign and malignant breast biopsies [22], suggesting that squamous lesions result in a similar mechanical manifestation as in adenomatous lesions. To preliminarily uncover the underlying mechanism, we assessed the expression of several molecular markers. Because all biopsies had to receive histopathological evaluation, we performed IHC staining instead of Western blotting to quantify their expression.

Previous studies reported that LEP reflected cell elasticity [22], while HEP was essentially the rigidity of ECM [36]. Hence, we speculated that the expression of Cdc42 (a cytoskeleton marker) and collagen I (the major ECM component) would change correspondingly. In agreement with this speculation, the IHC expression demonstrated specific Cdc42 upregulation in the HSIL group and increased collagen I in the cancer group, which exactly mirrored the variation tendency of the HSIL LEP and cancer HEP, respectively. To add further credence, we performed a novel analysis to explore whether there was a correlation between indexes of mechanics and molecular expression. Encouragingly, both Cdc42 and collagen I expression tended to be associated with LEP and HEP locations when the

Pearson correlation coefficient of collagen I with HEP reached 0.88. Collectively, these data indicate that the higher Cdc42 level in the HSIL group contributed to its LEP upshift, while the increased collagen I composition of the ECM resulted in cancer HEP transitions.

The importance of our study is not simply confined to the determination of nanomechanical properties of cervical cancers and precancerous lesions; our findings also have biological implications. First, cell elasticity within HSIL tissues was higher than in controls, and their biological behaviors were much more aggressive than in controls. Because cytoskeleton marker Cdc42 is associated with cell migration, invasiveness [40,41], and apoptosis [42], it was entirely possible that decreased cell compliance within the HSIL tissues was one of the causes of their progressive cancerous behaviors. Furthermore, cervical cancers have distinguished clinical prognosis and elasticity distribution simultaneously, which could potentially help in cancer diagnosis. Finally, it was recently reported that forces originating from the tumor facilitate its invasion [43]. In this study, we provide evidence supporting that ECM with increased rigidity can enhance cancer progression. Although these implications are encouraging, the definite biological significance of these findings needs further study.

There are some limitations in this study. First, unlike Western blotting, IHC staining is only a semi-quantitative method to determine protein expression [44,45]. In fact, we had no better choice to retain the integrity of the tissue organization. In addition, we used the index IOD/area [30,31] and mean values of 5 randomly chosen fields to minimize local staining biases. Second, the findings of correlation analysis are usually less reliable than those of molecular biological assays in mechanism studies. A molecular function assay using cell lines is the preferred option, despite the possibility that cancer cell lines

in vitro might not behave exactly as cancer cells *in vivo* [46]. Considering the difficulty in designing holistic function experiments (especially for collagen I), we regarded correlation analysis as an acceptable alternative. Third, we excluded samples with 1 peak or more than 2 peaks from the correlation analysis. Only 15 cases with 2 peaks (and only 2 peaks) were included. This would certainly decrease the efficacy of the correlation analysis, although it was an inevitable compromise for elasticity peak identification.

Conclusions

We resolved the nanomechanical signature of cervical biopsies at various disease stages from cervicitis to cervical cancer. To

References:

- Vaccarella S, Lortet-Tieulent J, Plummer M et al: Worldwide trends in cervical cancer incidence: Impact of screening against changes in disease risk factors. *Eur J Cancer*, 2013; 49: 3262-73
- Zhang Q, Xie W, Wang F et al: Epidemiological investigation and risk factors for cervical lesions: Cervical cancer screening among women in rural areas of Henan province China. *Med Sci Monit*, 2016; 22: 1858-65
- Schiffman M, Castle PE, Jeronimo J et al: Human papillomavirus and cervical cancer. *Lancet*, 2007; 370: 890-907
- Crum CP, McLachlin CM: Cervical intraepithelial neoplasia. *J Cell Biochem Suppl*, 1995; 23: 71-79
- Andrae B, Kemetli L, Sparén P et al: Screening-preventable cervical cancer risks: Evidence from a nationwide audit in Sweden. *J Natl Cancer Inst*, 2008; 100: 622-29
- Ingber DE, Dike L, Hansen L et al: Cellular tensegrity: Exploring how mechanical changes in the cytoskeleton regulate cell-growth, migration, and tissue pattern during morphogenesis. *Int Rev Cytol*, 1994; 150: 173-224
- Park CC, Bissell MJ, Barcellos-Hoff MH: The influence of the microenvironment on the malignant phenotype. *Mol Med Today*, 2000; 6: 324-29
- Wirtz D, Konstantopoulos K, Searson PC: The physics of cancer: The role of physical interactions and mechanical forces in metastasis. *Nat Rev Cancer*, 2011; 11: 512-22
- Hochmuth RM: Micropipette aspiration of living cells. *J Biomech*, 2000; 33: 15-22
- Gardel ML, Shin JH, MacKintosh FC et al: Elastic behavior of cross-linked and bundled actin networks. *Science*, 2004; 304: 1301-5
- Guilluy C, Osborne LD, Van Landeghem L et al: Isolated nuclei adapt to force and reveal a mechanotransduction pathway in the nucleus. *Nat Cell Biol*, 2014; 16: 376-81
- Rebelo LM, de Sousa JS, Mendes Filho J, Radmacher M: Comparison of the viscoelastic properties of cells from different kidney cancer phenotypes measured with atomic force microscopy. *Nanotechnology*, 2013; 24: 055102
- Zhou Z, Zheng C, Li S et al: AFM nanoindentation detection of the elastic modulus of tongue squamous carcinoma cells with different metastatic potentials. *Nanomedicine*, 2013; 9: 864-74
- Cross SE, Jin YS, Rao J, Gimzewski JK: Nanomechanical analysis of cells from cancer patients. *Nat Nanotechnol*, 2007; 2: 780-83
- Lekka M, Gil D, Pogoda K et al: Cancer cell detection in tissue sections using AFM. *Arch Biochem Biophys*, 2012; 518: 151-56
- Park S: Nano-mechanical phenotype as a promising biomarker to evaluate cancer development, progression, and anti-cancer drug efficacy. *J Cancer Prev*, 2016; 21: 73-80
- Lekka M, Laidler P, Gil D et al: Elasticity of normal and cancerous human bladder cells studied by scanning force microscopy. *Eur Biophys J*, 1999; 28: 312-16
- Xu W, Mezencev R, Kim B et al: Cell stiffness is a biomarker of the metastatic potential of ovarian cancer cells. *PLoS One*, 2012; 7: e46609
- Zhao X, Zhong Y, Ye T et al: Discrimination between cervical cancer cells and normal cervical cells based on longitudinal elasticity using atomic force microscopy. *Nanoscale Res Lett*, 2015; 10: 482
- Ding YX, Cheng Y, Sun QM et al: Mechanical characterization of cervical squamous carcinoma cells by atomic force microscopy at nanoscale. *Med Oncol*, 2015; 32: 71
- Weder G, Hendriks-Balk MC, Smajda R et al: Increased plasticity of the stiffness of melanoma cells correlates with their acquisition of metastatic properties. *Nanomedicine*, 2014; 10: 141-48
- Plodinec M, Loparic M, Monnier CA et al: The nanomechanical signature of breast cancer. *Nat Nanotechnol*, 2012; 7: 757-65
- Tian M, Li Y, Liu W et al: The nanomechanical signature of liver cancer tissues and its molecular origin. *Nanoscale*, 2015; 7: 12998-3010
- O'Neill CJ, McCluggage WG: p16 expression in the female genital tract and its value in diagnosis. *Adv Anat Pathol*, 2006; 13: 8-15
- Erickson JW, Cerione RA: Multiple roles for Cdc42 in cell regulation. *Curr Opin Cell Biol*, 2001; 13: 153-57
- Danforth DN: The fibrous nature of the human cervix, and its relation to isthmic segment in gravid and non gravid uteri. *Am J Obstet Gynecol*, 1947; 53: 541-60
- Iwahashi M, Muragaki Y, Ooshima A, Umehashi N: Decreased type I collagen expression in human uterine cervix during pregnancy. *J Clin Endocrinol Metab*, 2003; 88: 2231-35
- Aspden RM: Collagen organisation in the cervix and its relation to mechanical function. *Coll Relat Res*, 1988; 8: 103-12
- Kaniewska E, Sielicka A, Sarathchandra P et al: Immunohistochemical and functional analysis of ectonucleoside triphosphate diphosphohydrolase 1 (CD39) and ecto-5'-nucleotidase (CD73) in pig aortic valves. *Nucleosides Nucleotides Nucleic Acids*, 2014; 33: 305-12
- Jia XL, Li SY, Dang SS et al: Increased expression of chondroitin sulphate proteoglycans in rat hepatocellular carcinoma tissues. *World J Gastroenterol*, 2012; 18: 3962-76
- Li Y, Wang W, Jia X et al: A targeted multiple antigenic peptide vaccine augments the immune response to self TGF- β 1 and suppresses ongoing hepatic fibrosis. *Arch Immunol Ther Exp (Warsz)*, 2015; 63: 305-15
- Petry KU: Management options for cervical intraepithelial neoplasia. *Best Pract Res Clin Obstet Gynaecol*, 2011; 25: 641-51
- Martin CM, O'Leary JJ: Histology of cervical intraepithelial neoplasia and the role of biomarkers. *Best Pract Res Clin Obstet Gynaecol*, 2011; 25: 605-15
- WHO Guidelines Approved by the Guidelines Review Committee. WHO Guidelines for Screening and Treatment of Precancerous Lesions for Cervical Cancer Prevention. Geneva: World Health Organization; 2013
- WHO Guidelines Approved by the Guidelines Review Committee. WHO Guidelines for Treatment of Cervical Intraepithelial Neoplasia 2-3 and Adenocarcinoma *in situ*: Cryotherapy, Large Loop Excision of the Transformation Zone, and Cold Knife Conization. Geneva: World Health Organization; 2014

Declaration of conflicting interest

The authors declare that they have no competing interests.

36. Levental KR, Yu H, Kass L et al: Matrix crosslinking forces tumor progression by enhancing integrin signaling. *Cell*, 2009; 139: 891–906
37. Ozkan AD, Topal AE, Dana A et al: Atomic force microscopy for the investigation of molecular and cellular behavior. *Micron*, 2016; 89: 60–76
38. Guz NV, Dokukin ME, Woodworth CD et al: Towards early detection of cervical cancer: Fractal dimension of AFM images of human cervical epithelial cells at different stages of progression to cancer. *Nanomedicine*, 2015; 11: 1667–75
39. Kuznetsova TG, Starodubtseva MN, Yegorenkov NI et al: Atomic force microscopy probing of cell elasticity. *Micron*, 2007; 38: 824–33
40. Ye H, Zhang Y, Geng L, Li Z: Cdc42 expression in cervical cancer and its effects on cervical tumor invasion and migration. *Int J Oncol*, 2015; 46: 757–63
41. Bustelo XR, Sauzeau V, Berenjano IM: GTP-binding proteins of the Rho/Rac family: regulation, effectors and functions *in vivo*. *Bioessays*, 2007; 29: 356–70
42. Wang J, Xu R, Wu J, Li Z: MicroRNA-137 negatively regulates H2O2-induced cardiomyocyte apoptosis through CDC42. *Med Sci Monit*, 2015; 21: 3498–504
43. Kopanska KS, Alcheikh Y, Staneva R et al: Tensile forces originating from cancer spheroids facilitate tumor invasion. *PLoS One*, 2016; 11: e0156442
44. Mulrane L, Rexhepaj E, Penney S et al: Automated image analysis in histopathology: A valuable tool in medical diagnostics. *Expert Rev Mol Diagn*, 2008; 8: 707–25
45. Rojo M G, Bueno G, Slodkowska J: Review of imaging solutions for integrated quantitative immunohistochemistry in the Pathology daily practice. *Folia Histochem Cytobiol*, 2009; 47: 349–54
46. Kim JB, Stein R, O'Hare MJ: Three-dimensional *in vitro* tissue culture models of breast cancer – a review. *Breast Cancer Res Treat*, 2004; 85: 281–91